The Astrophysical Journal, 693:L39–L43, 2009 March 1 doi:10.1088/0004-637X/693/1/L39

CARBON MONOXIDE IN THE CASSIOPEIA A SUPERNOVA REMNANT

J. Rho[1], T. H. Jarrett[1], W. T. Reach[1], H. Gomez[2], and M. Andersen[1]
[1] *Spitzer* Science Center, California Institute of Technology, Pasadena, CA 91125, USA; rho@ipac.caltech.edu, jarrett@ipac.caltech.edu, reach@ipac.caltech.edu, mortena@ipac.caltech.edu
[2] School of Physics and Astronomy, Cardiff University, The Parade, Cardiff CF24 3AA, UK; gomez@astro.cf.ac.uk
Received 2008 October 8; accepted 2009 January 14; published 2009 February 16

ABSTRACT

We report the likely detection of near-infrared 2.29 μm first overtone carbon monoxide (CO) emission from the young supernova (SN) remnant Cassiopeia A (Cas A). The continuum-subtracted CO filter map reveals CO knots within the ejecta-rich reverse shock. We compare the first overtone CO emission with that found in the well studied supernova SN 1987A and find ∼30 times less CO in Cas A. The presence of CO suggests that molecule mixing is small in the SN ejecta and that astrochemical processes and molecule formation may continue at least ∼ 300 yr after the initial explosion.

Key words: dust, extinction – ISM: molecules – supernova remnants – supernovae: general

1. INTRODUCTION

Supernovae (SNe) are suggested to be the first molecular factories in the early Universe (Cherchneff & Lilly 2008). Molecules such as carbon monoxide (CO) are sensitive diagnostics of the temperature, density, and degree of mixing in the SN ejecta. Understanding the chemistry within the ejecta, and the abundance and mixing of CO and SiO molecules, is particularly important in studying dust formation processes since this controls how much carbon is available to form amorphous carbon grains and how much oxygen is available beyond that bound in CO and SiO molecules to form $MgSiO_3$ and Mg_2SiO_4. The existence of CO in SN ejecta suggests that dust formation can occur, since molecules are indicative of relatively cool ejecta (typically few thousand degrees). CO itself is an effective coolant (Liu & Dalgarno 1995), so that once it forms it could enhance dust formation. Isotopic compositions of meteoric dust grains (Clayton & Nittler 2004) show that carbon-rich dust is condensed within the interior of SN ejecta. In O-rich ejecta, radioactivity and mixing processes produce "free" carbon in which to form dust.

The *quantity* of dust formed within SNe ejecta has become a subject of debate in recent years (see Rho et al. 2008 and references therein; Dunne et al. 2009). Lagage et al. (1996) first showed evidence, in *Infrared Space Observatory* (*ISO*) images, for dust formation in the nearby, young supernova remnant (SNR) Cas A. Rho et al. (2008) identified three distinct ejecta dust populations based on their continuum shapes in *Spitzer Space Telescope* spectra, including broad features peaking at 21 μm, and estimated a total dust mass of between 0.02 and 0.054 $M_\odot$. These observations provide definitive evidence of freshly formed dust in a young SNR and show that SNe are important dust contributors to the large quantities of dust observed at high redshifts. Theoretical models (Todini & Ferrara 2001; Nozawa et al. 2003; Bianchi & Schneider 2007) predict a dust mass of 0.3–1 $M_\odot$ per SN. However, our current understanding of dust chemistry and composition is limited. The current models assume that very little carbon is locked up in CO and almost all of the carbon is available for dust formation. The results from dust evolution models therefore depend significantly on the C/O ratio in the gas (see Morgan & Edmunds 2003; Dwek et al. 1998).

Images obtained with the *Spitzer* Infrared Array Camera (IRAC) each present a different view of the nucleosynthesis within Cas A (Ennis et al. 2006). A surprising result from the IRAC observations is the similarity between the morphology of the IRAC Band 2 image (centered at 4.5 μm) and ejecta-dominated images of the remnant. The origin of this emission is not known, but based on the lack of bright Hα emission, the contribution from Brα emission is likely small. Ennis et al. (2006) therefore suspected that CO emission was responsible for the emission at this wavelength, but this could not be confirmed since the *Spitzer* Infrared Spectrograph (IRS) has a blue cutoff of 5.2 μm.

As a tracer of gas properties and dust formation, CO is potentially an important diagnostic for any SN. The first detection of CO from supernova ejecta was from the well studied, Type II supernova SN1987A (Catchpole et al. 1989; Meikle et al. 1989; Spyromilio et al. 1988), providing a unique insight into the chemical dynamics of the explosion and ejecta. The variation of the observed CO emission with time after the initial explosion was modeled by Spyromilio et al. (1988), who suggested that CO formed out in the SN ejecta at a temperature of 1800 K and expansion velocity 1200 km s^{-1} 337 days after the explosion. They determined a total mass $M_{CO} \sim 10^{-3}$ $M_\odot$. Spyromilio & Leibundgut (1996) detected $\sim 10^{-3}$ $M_\odot$ of CO forming at temperature 4000 K in SN 1995ad. CO has further been detected from the Type IIn SN 1998S (Gerardy et al. 2001), SN 2002dh (Pozzo et al. 2006), and the Type Ic SN 2000ew (Gerardy et al. 2002). The number of CO detections in SNe in the literature is still relatively small, and all are restricted to within a few years after the initial explosion. In this Letter, we report the likely detection of the CO overtone from Cas A, an approximately 300 yr old SNR. This is the first time CO emission has been detected in a Galactic SNR and suggests that molecule formation is not only a common occurrence in core-collapse ejecta but molecules also exist (or continue forming) long after the initial explosion event.

2. OBSERVATIONS

We observed Cas A on 2006 September 3 and 4 with the Wide field InfraRed Camera (WIRC, Wilson et al. 2003) on the Hale 200 inch (5 m) telescope at Mount Palomar. The weather was very clear with the seeing typically 0.″8. The camera field of

Figure 1. Mosaicked color image of Cas A with WIRC, with CO (red), *K*-continuum (green) and Pβ (blue). The range of surface brightnesses measured from the diffuse structures are 0.31–2.79 $\times$ 10^{-5} for CO, 0.23–1.4 $\times$ 10^{-5} for *K*-continuum, and 1.2–29.0 $\times$ 10^{-5} erg s^{-1} cm^{-2} sr^{-1} for Pβ. CO-excess regions (in red) are marked as boxes (the bottom box marks the location of the Minkowski knot). The image is centered at R.A. 350.°858 and decl. 58.°814 (J2000), and covers an $7' \times 7'$ arcmin field of view.

view is 8.″7. We observed a set of dithered positions (designed to uniformly cover the supernova remnant), with interleaved, dithered observations of an "off" position 30′ away. A sky reference image was generated from the "off" images, and was subtracted from the "on" images after scaling to match the median sky brightness. This observation and analysis procedure preserved the diffuse emission of the SNR. We took narrowband images using filters centered on CO(2–0) at 2.294 μm, *K*-band and *H*-band continuum at 2.270 and 1.570 μm, and Pβ at 1.182 μm (see Figure 1). The narrowband filter widths are typically 0.025 μm. The exposure time of CO, *K*-cont, and Pβ is a combined 90 s from three back-to-back images of 30 s exposure (to reduce the number of saturated stars), with a total on-source integration time of 8100 s for CO, 7290 s for *K*-cont, and 810 s for Pβ. The exposure time of *H*-cont is 90 s, with a total on-source integration time of 1440 s. Respective sensitivities of the narrow-filter images are 1.70×10^{-6} erg s^{-1} cm^{-2} sr^{-1} for CO, 1.04 $\times$ 10^{-6} for *K*-cont, 1.54×10^{-6} for *H*-cont, and 1.25 $\times$ 10^{-5} for Pβ. The detailed data reduction methods are similar to those described in Keohane et al. (2007); additionally, focal plane distortion was derived from the images and corrected. We directly subtracted the *K*-continuum image from the CO filter image in order to subtract stars and contamination from synchrotron emission from Cas A (Rho et al. 2003). Due to excellent seeing (0.″8) and low air mass toward Cas A, the stars were well subtracted. We further masked saturated stars and applied adaptive smoothing and wavelet filtering to the images.

3. RESULTS

Figure 1 shows a color composite image of Cas A, combining the Pβ line (blue), 2.27 μm continuum (green), and CO (2–0) 2.29 μm line (red). Pβ traces recombining atomic hydrogen. The 2.27 μm continuum consists mostly of nonthermal synchrotron radiation and delineates the shell structure (see Rho et al. 2003). Finally, the CO (2–0) overtone emission traces the dense knots of gas along the shell and interior interface. The molecular emission is evident as red in Figure 1 and more easily seen in the continuum-subtracted CO image, Figure 2, revealing the line emission toward the northern parts of bright rings and an eastern filament of the Minkowski knots in the southeast. The CO emission is highly clumpy and distributed in a collection of knots with an upper limit on the size of $\sim$ 0.013 pc (limited by the spatial resolution of 0.″8) at a distance $3.4^{+0.3}_{-0.1}$ kpc (Reed et al. 1995). The flux densities for the dense gas knots are listed in Table 1. We selected the brightest knots of

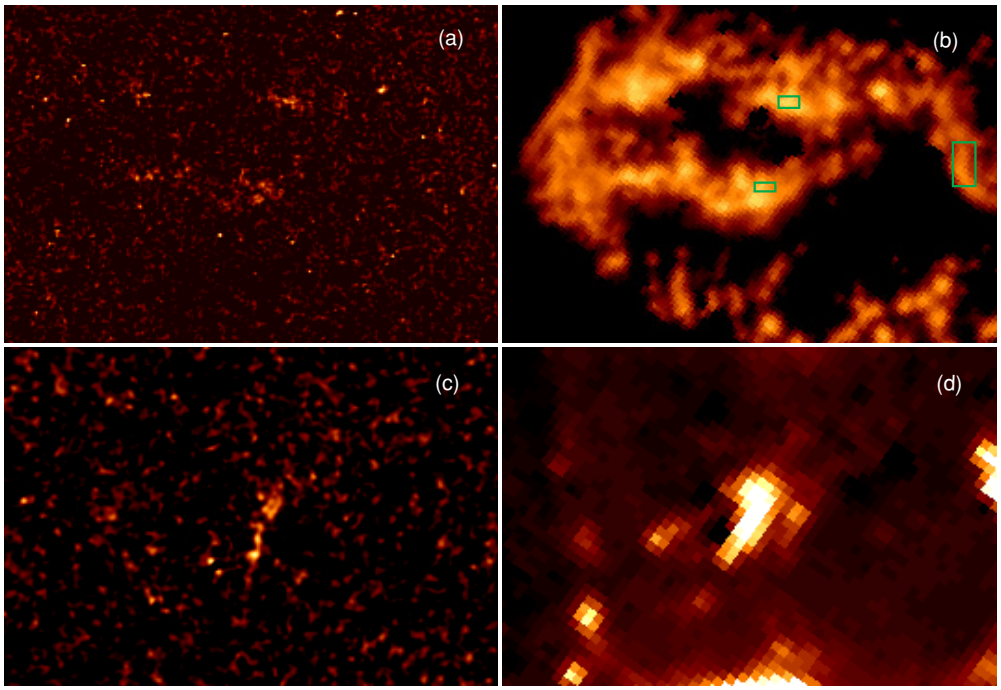

Figure 2. Zoomed-in continuum-subtracted CO ((a) and (c)) and IRAC2 ((b) and (d)) color images toward CO-detected regions. These zoomed-in images cover the regions marked as boxes in Figure 1: the panels (a) and (b) show the northern bright ring (centered at R.A. 350.°857 and decl. 58.°836 (J2000), with area 2.′5 × 1.′2), and panels (c) and (d) are toward the Minkowski knots (centered at R.A. 350.°888 and decl. 58.°802 (J2000), with area 1.′2 × 0.′6), respectively. The near-infrared CO images (a) and (c) include the CO (2–0) first overtone, and the *Spitzer* IRAC 2 images (b) and (d) include the CO (1–0) fundamental. The locations of the three knots in Table 1 are marked as green rectangles (upper: CO knot1; lower: CO knot2; and right: NW knot).

18 regions in the CO, *K*-continuum, or Pβ images with angular sizes 3″–15″ and estimated the flux densities after background subtraction. The regions include knots which are bright in the continuum-subtracted CO image and the flux densities of individual knots range from 0.1 to 0.3 mJy. The flux densities of two representative CO knots and one other knot in the NW are given in Table 1 along with the positions. The total flux density of the CO-detected area after *K*-continuum subtraction (see Figures 2(a) and (c)), is 1.27 ± 0.17 mJy, where the estimated error includes calibration (7%), background variation (5%), and statistical (10%) errors. Some faint, diffuse CO emission from Cas A may have been removed from our image because of the continuum subtraction; the flux reported here is conservative, including only the bright knots. After extinction correction using A_v of 4.5 mag (Fesen & Gunderson 1996) and the extinction law of Rieke & Lebofsky (1985), the flux density is 2.03 ± 0.27 mJy, equivalent to a CO overtone luminosity of 0.01 ± 0.0014 $d_{3.4\mathrm{kpc}}\ L_{\odot}$. The ratio of *H*-continuum to *K*-continuum is globally consistent with the origin of synchrotron radiation with a synchrotron index of 0.65–0.71 (Rho et al. 2003); moreover, the *H*-continuum and *K*-continuum images are similar to the radio image (Wright et al. 1999; Rho et al. 2003), indicating they are dominated by synchrotron emission.

We compiled spectral energy distributions (SEDs) of near-infrared *H* and *K* bands, and *Spitzer* IRAC bands 1–3 (3.6–5.8 μm) bands for 18 knots; Figure 3 shows three representative SEDs after correcting for the extinction. The SEDs show a sudden jump at 2.294 μm toward the CO detection positions, with no such jump toward the NW ejecta position. The SEDs of the CO knots also show a larger IRAC Band 2 (4.5 μm) excess than that of the NW ejecta knot.

A few knots toward Pβ emitting regions (blue in Figure 1) show *K*-continuum brighter than the CO-band emission. These knots look like elliptical spheroids, indicative of Quasi-Stationary Flocculi (Fesen & Gunderson 1996, Willingale et al. 2002). We further note that *H*-continuum emission toward hydrogen knots is slightly higher than that expected from synchrotron emission, suggesting that despite the narrow bandwidth of the *H*-continuum filter, the image may be picking up the weak hydrogen line Brλ at 1.57 μm. The CO filter does not include any hydrogen or helium lines. The near-infrared spectra of Gerardy et al. (2001) did not detect any hydrogen and helium lines within the *H*-cont, *K*-cont, CO filters, but our images have a higher sensitivity and therefore may be detecting such lines.

The Pβ emission is largely from shocked circumstellar gas, and similar to the optical Hα emission (Fesen & Gunderson 1996; Fesen 2001). The emission is mainly clustered in the northernmost inner shell and outside the southwestern shell, as shown in Figure 1. The former contains both circumstellar gas and fast moving knots. The hydrogen lines of circumstellar medium knots also show moderate high-velocity components, which are defined as "mixed emitting knots" by Fesen & Gunderson (1996), who discussed their origin. In particular, rich infrared ejecta emission is detected from the northernmost inner shell (see Figure 2 of Rho et al. 2008). Fesen & Gunderson (1996) suggested that mixed emitting knots may be "splatter" fragments produced as high speed underlying core condensations broke through and partially mixed with the progenitor star's surface layers.

4. DISCUSSION

We detected significant near-infrared CO overtone emission from small portions of the Cas A remnant toward the northern part of the bright ring and in the eastern region of Minkowski knots in the southeast. It is possible that we are missing fainter CO emission elsewhere in the SNR due to our detection limit (of 1.98×10^{-6} erg s^{-1} cm^{-2} sr^{-1}) in the continuum-subtracted

Table 1
Summary of Observed Brightnesses

Filter	Flux Density[a]	Flux Density (mJy)		
	Range	CO Knot1[b]	CO Knot2[b]	NW Knot[b]
2.27 μm (*K*-cont)	0.1−1.0	0.610 ± 0.009	0.290 ± 0.006	1.780 ± 0.016
2.29 μm (CO)	0.2−1.2	0.850 ± 0.013	0.490 ± 0.010	1.880 ± 0.020
3.6 μm (IRAC 1)	0.4−2.3	0.71 ± 0.20	0.38 ± 0.16	2.23 ± 0.35
4.5 μm (IRAC 2)	1.2−15.0	11.03 ± 0.64	5.10 ± 0.45	9.24 ± 0.60
5.8 μm (IRAC 3)	0.6−4.2	2.20 ± 0.42	1.04 ± 0.34	3.05 ± 0.67

Notes.
[a] The range of flux densities (in mJy) toward CO detected positions.
[b] Positional coordinates in R.A. and Decl. (J2000): CO knot1 (green in Figure 3) at 350.°850, 58.°840; knot2 (red) at 350.°854, 58.°834; and the northwest ejecta knot (blue) at 350.°825 and 58.°836. The flux densities were measured by averaging over an angular size of 5.″3 × 3.″1, 38″ × 10″, and 6″ × 12″ for knot1, knot2, and the NW knot, respectively.

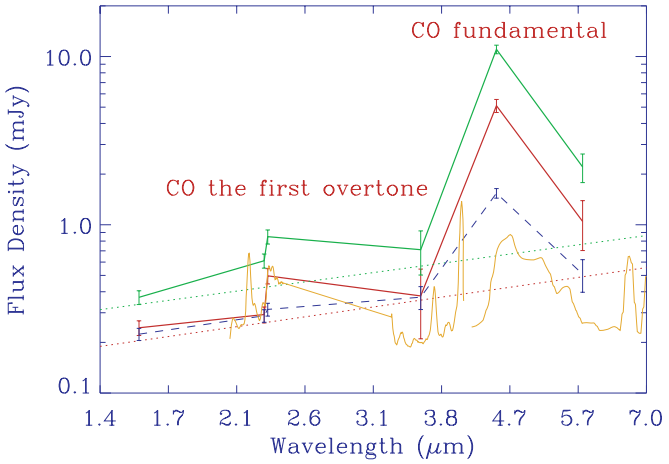

Figure 3. Spectral energy distribution of two representative CO emitting knots: knot1 (green) and knot2 (red) (positions are given in Table 1) which show excess emission at 2.294 μm. The contribution from the synchrotron continuum is shown by the dotted line. Comparison with the SED (scaled to the CO knot1 continuum) of the NW ejecta knot (blue dashed curve) shows that the knots with near-infrared CO-filter excess emission may also contain the CO fundamental emission in the IRAC band 2. The error bars of near-infrared emission include both statistical and calibration errors. The SN 1987A spectrum is shown for comparison (orange curve) at 255–260 d after the explosion event (courtesy of Peter Meikle, Meikle et al. 1989; Wooden et al. 1993).

CO image. The locations where CO emission is detected coincide with the ejecta at the reverse shock (Hwang et al. 2004; Fesen & Gunderson 1996; Rho et al. 2008; Yang et al. 2009). This indicates that the CO gas was formed in the ejecta.

The *Spitzer* IRAC Band 2 image shows a morphology similar to ejecta-dominated images, but the origin of this emission was a mystery. After scaling from the overtone to the fundamental band, our observations suggest that the CO fundamental contributes some (greater than 1/6) but possibly not all of the emission in IRAC Band 2 (Figure 3). Other contributors to this band include multiple [Fe II], hydrogen recombination and helium lines. The ratios of IRAC 2 and CO-filter emission from 18 knots across Cas A suggest that CO contributes 10–30% of the emission in the CO emitting regions when compared with non-CO emitting ejecta knots. Constraining the percentage of CO contribution to the IRAC band 2 image is difficult since the ratio of the fundamental to the first overtone varies depending on the ejecta temperature and density. We cannot therefore strongly constrain the CO contribution to the IRAC Band 2. We analyzed the IRS spectroscopy cube to find any signature of the fundamental CO (4.8–6 μm), but the signal-to-noise was too poor. The *Spitzer* IRS data are not sensitive enough to detect this emission (errors of the IRS spectra were 1–2 MJy sr^{-1}, an order of magnitude higher than the typical flux densities of near-infrared CO emission) although there might be some hint for the northern position (at the position of the strongest 21 μm dust spectrum). We also looked for SiO molecules (at 8–10 μm), but could not distinguish them from the silicate emission feature at 9.8 μm (silicate stretching mode).

We estimated the mass of CO in Cas A by comparing the CO flux density in Cas A with that found in SN 1987A, since without spectra it is not possible to derive a density, temperature, and velocity of CO gas. Figure 3 compares the CO emission from Cas A and SN 1987A (Meikle et al. 1989; Wooden et al. 1993). After accounting for the distance differences, the CO (2–0) first overtone flux density of Cas A is a factor of $\sim$ 28 smaller than that of SN1987A on day 255. Assuming the same gaseous conditions as seen in the CO emitting regions in SN1987A (a temperature of 1800–2800 K and a velocity of 2000 km s^{-1}), we estimated the CO mass in Cas A to be $M_{\rm CO} \sim 1.7 \times 10^{-6}\ M_{\odot}$ for Local Thermodynamic Equilibrium (LTE) (Spyromilio et al. 1988) and $8.2 \times 10^{-6}\ M_{\odot}$ for non-LTE (Liu et al. 1992). Note that the CO mass estimate is highly uncertain because we assume the gas properties described above.

The CO detections in SNe have been within a few years after the initial explosion. The main destruction process of CO is from impacts with energetic electrons (Liu et al. 1992) and with ionized gas atoms. The latter process quickly destroys CO, hence the detection of the CO fundamental band provides constraints on the degree of mixing in the SN ejecta. Given that Cas A is believed to be the remnant of a Type IIb explosion (Krause et al. 2008), this suggests that either the CO layer is not macroscopically mixed with ionized helium or that the helium is not ionized. The typical electron density of C- and O-rich regions during formation of CO is shown to be 5×10^8 cm^{-3} (Gearhart et al. 1999). The highly clumpy structures can be explained by such high-density CO gas within the warm or hot ejecta, which naturally fortifies the evidence of fresh dust formation observed in Cas A (Lagage et al. 1996; Rho et al. 2008).

In dust evolution models, understanding CO molecules in SN ejecta is a key physical question. The formation efficiency of CO molecules critically affects the dust formation efficiency. In chemical equilibrium, the abundance of CO is balanced between radiative processes and radioactive decay of ^{56}Co, because the main destruction process is by the energetic electrons produced by the radioactive decay of ^{56}Co (Liu et al. 1992; Clayton et al. 2001). Both Nozawa et al. (2003) and Todini & Ferrara (2001) assumed the mass fraction of C atoms that are not locked in CO is 99–100%, and Travaglio et al. (1999) assumed that mixing occurs at the molecular level, prior to dust condensation. In contrast, Clayton & Nittler (2004), Deneault et al. (2003), and Fryxell et al. (1991) suggest that gases are unlikely to be mixed at the molecular level within a few years. Our CO detection suggests that molecular mixing is small (at least smaller than previously thought) in the SN ejecta and during the development of the reverse shock. CO molecules in Cas A suggest a higher CO abundance in the gas phase and lower efficiency in dust formation of carbon dust. Remaining molecules also indicate that dust formation was inefficient (leaving molecular leftovers) or occurred inhomogeneously (e.g., only in dense knots). Deep infrared spectroscopic observations will allow us to measure the velocity, temperature, and density of the CO molecules in Cas A and to study the ongoing chemistry of molecules in SN ejecta.

5. CONCLUSIONS

We detected CO emission from the young SNR Cas A. This may be the first CO detection from an older SN (age ∼300 yr). CO emission has also been detected in eight other core-collapse remnants, but in all cases it has been limited to within three years of the explosion. Theoretical models suggest that dust formation in SNe occurs between 200–800 d after the SN event yet the observations presented here suggest that molecular and dust formation processes could continue long after. The detection of CO in the Cas A remnant demonstrates that astrochemical processes are still ongoing more than 300 yr after the initial explosion.

We are grateful to Achim Tappe who participated in the Palomar observing run, and thank Takashi Onaka for fruitful discussion on dust and CO formation. We also thank Palomar Observatory staff (Jean Mueller, Jeff Hickey, and Karl Dunscombe) for assistance during our observing runs. We thank the anonymous referee for careful reading and helpful comments. H. Gomez would like to thank Las Cumbres Observatory for its support. M. Andersen is partially supported by NASA through LTSA grant NRA-01-01-LTSA-013. Based on observations obtained at the Hale Telescope, Palomar Observatory, as part of a continuing collaboration between the California Institute of Technology, NASA/JPL, and Cornell University.

REFERENCES

Bianchi, S., & Schneider, R. 2007, MNRAS, 378, 973
Catchpole, et al. 1989, MNRAS, 237, 55
Cherchneff, I., & Lilly, S. 2008, ApJ, 683, L123
Clayton, D. D., Deneault, E. A.-N., & Meyer, B. S. 2001, ApJ, 562, 480
Clayton, D. D., & Nittler, L. R. 2004, ARA&A, 42, 39
Deneault, E. A.-N., Clayton, D. D., & Heger, A. 2003, ApJ, 594, 312
Dunne, L., et al. 2009, MNRAS, in press (arXiv:0809.0887)
Dwek, E. 1998, ApJ, 501, 643
Dwek, E., et al. 2008, ApJ, 676, 1029
Ennis, J., Rudnick, L., Reach, W. T., Smith, J. D., Rho, J., DeLaney, T. D., Gomez, H., & Kozasa, T. 2006, ApJ, 652, 376
Fesen, R. A. 2001, ApJS, 133, 161
Fesen, R. A., & Gunderson, K. S. 1996, ApJ, 470, 967
Fryxell, B., Arnett, D., & Mueller, E. 1991, ApJ, 367, 619
Gearhart, R. A., Wheeler, J. C., & Swartz, D. A. 1999, ApJ, 510, 944
Gerardy, C. L., & Fesen, R. A. 2001, AJ, 121, 2781
Gerardy, C. L., Fesen, R. A., Hoflich, P., & Wheeler, J. C. 2000, AJ, 119, 2968
Gerardy, C. L., Fesen, R. A., Nomoto, K., Meada, K., Hoflich, P., & Wheeler, J. C. 2002, PASJ, 54, 905
Hwang, U., et al. 2004, ApJ, 615, 117
Keohane, J. W., Reach, W. T., Rho, J., & Jarrett, T. H. 2007, ApJ, 654, 938
Kozasa, T., Hasegawa, H., & Nomoto, K. 1991, A&A, 249, 474
Kotak, R., et al. 2006, ApJ, 651, L117
Krause, O., Birkmann, S. M., Usuda, T., Hattori, T., Goto, M., Reike, G. H., & Misselt, K. A. 2008, Science, 320, 1195
Lagage, P. O., Claret, A., Ballet, J., Boulanger, F., Cesarsky, C. J., Cesarsky, D., Fransson, C., & Pollock, A. 1996, A&A, 315, L273
Liu, W., & Dalgarno, A. 1995, ApJ, 454, L472
Liu, W., Dalgarno, A., & Lepp, S. 1992, ApJ, 396, L679
Maiolino, R., et al. 2006, Mem. Soc. Astron. Ital., 77, 643
Meikle, W. P. S., Spyromilio, J., Varani, G.-F., & Allen, D. A. 1989, MNRAS, 238, 193
Morgan, H. L., & Edmunds, M. G. 2003, MNRAS, 343, 427
Nozawa, T., Kozasa, T., Umeda, H., Maeda, K., & Nomoto, K. 2003, ApJ, 598, 785
Pozzo, M., et al. 2006, MNRAS, 368, 1169
Reed, J. E., Hester, J. J., Fabian, A. C., & Winkler, P. F. 1995, AJ, 440, 706
Rho, J., Reynolds, S., Reach, W., Jarrett, T., Allen, G., & Wilson, J. 2003, ApJ, 592, 299
Rho, J., et al. 2008, ApJ, 673, 271
Rieke, G. H., & Lebofsky, M. J. 1985, ApJ, 288, 618
Spyromilio, J., & Leibundgut, B. 1996, MNRAS, 283, L89
Spyromilio, J., Meikle, W. P. S., Learner, R. C. M., & Allen, D. A. 1988, Nature, 334, 327
Todini, P., & Ferrara, A. 2001, MNRAS, 325, 726
Travaglio, C., Gallino, R., Amari, S., Zinner, E., Woosley, S., & Lewis, R. S. 1999, ApJ, 510, 325
Willingale, R., Bleeker, J. A. M., van der Heyden, K. J., Kaastra, J. S., & Vink, J. 2002, A&A, 381, 1039
Wilson, J. C., et al. 2003, Proc. SPIE, 4841, 451
Wooden, D. H., et al. 1993, ApJS, 88, 477
Wright, M., Dickel, J., Koralesky, B., & Rudnick, L. 1999, ApJ, 518, 284
Yang, X. J., Tsunemi, H., Lu, F. J., & Chen, L. 2009, ApJ, in press (arXiv:0810..4687)